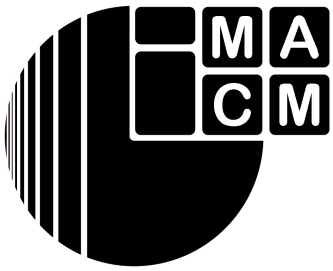

Bergische Universität Wuppertal

Fachbereich Mathematik und Naturwissenschaften

Institute of Mathematical Modelling, Analysis and Computational Mathematics (IMACM)

Preprint BUW-IMACM 19/10

A. Liefke, V. Marciniak, J. Backhaus, C. Frey, H. Gottschalk and U. Janoske

Aerodynamic Impact of Manufacturing Variation on a Nonaxisymmetric Multi-Passage Turbine Stage with Adjoint CFD

March 20, 2019

http://www.math.uni-wuppertal.de

AERODYNAMIC IMPACT OF MANUFACTURING VARIATION ON A NONAXISYMMETRIC MULTI-PASSAGE TURBINE STAGE WITH ADJOINT CFD

Alexander Liefke*
Siemens AG, Power and Gas
Mülheim an der Ruhr
45473, Germany
alexander.liefke@siemens.com

Vincent Marciniak
Siemens AG, Power and Gas
Mülheim an der Ruhr
45473, Germany
vincent.marciniak@siemens.com

Jan Backhaus
Institute of Propulsion Technology
German Aerospace Center (DLR)
Köln, 51147 , Germany
jan.backhaus@dlr.de

Christian Frey
Institute of Propulsion Technology
German Aerospace Center (DLR)
Köln, 51147 , Germany
christian.frey@dlr.de

Hanno Gottschalk
School of Mathematics and Science
University of Wuppertal
Wuppertal, 42119, Germany
hanno.gottschalk@uni-wuppertal.de

Uwe Janoske
Chair of Fluid Mechanics
University of Wuppertal
Wuppertal, 42119, Germany
uwe.janoske@uni-wuppertal.de

ABSTRACT

Turbomachinery blade design is based on an axisymmetric model assuming identical blades in the circumferential direction. The blade manufacturing process, however, has a finite accuracy leading to surface imperfections and therefore non-identical blades. This leads to a variation in each passage cross area effecting the aerodynamic performance of the turbine.

The simulation of multiple 3D CFD blade passages, nevertheless, is still computational expensive. However, if the effect of nonaxisymmetric blades is small enough to be approximated as linear, the adjoint method is an inexpensive alternative, which can be used in an industrial context. A set of 102 turbine vanes is used to model the manufacturing variations and assess the aerodynamic impact of up to eight nonaxisymmetric blade passages of a transonic high pressure turbine stage.

It is shown that the modeled blade passage results superimpose linearly. Therefore, the aerodynamic impact of surface imperfections can be evaluated by superpositioning the single-passage results, which are generated by an adjoint computation.

NOMENCLATURE

[30mm] A area
AD Algorithmic differentiation
CFD Computational Fluid Dynamics
CLT Central Limiting Theorem
FEM Finite Element Method
H Total Enthalpy
MVs Manufacturing Variations
n Number of Blades
p Number of Passages
RANS Reynolds Averaged Navier Stokes
v Velocity
$\dot{m}$ Mass Flow
η Isentropic Efficiency
ρ Density
μ Mean Value
σ Standard Deviation

INTRODUCTION

Surface imperfections of turbomachinery blades are caused by the finite accuracy of the manufacturing process. A turbomachinery blade row, hence, never consists of identical blades. This, however, contradicts the axisymmetric design approach assuming identical blades in circumferential direction. An assessment of the aerodynamic performance scatter would therefore re-

*Address all correspondence to this author.

quire nonaxisymmetric modeling to evaluate the impact of manufacturing variations (MVs).

A first approach with nonaxisymmetric modeling for the rotor of a 1.5-stage compressor is presented by Lange et al. [1]. The authors analyze 150 optical rotor blade scans to take into account the aerodynamic impact of MVs with up to eight rotor passages using RANS computations. This study concludes that a single passage evaluation overestimates the aerodynamic scatter. Lange et al. show that the aerodynamic scatter for a full annulus configuration reduces by 87% compared to a single passage.

Another approach is presented by Lejon et al. [2] who analyze the aerodynamic impact of a compressor blisk with 23 blades applying full annulus RANS evaluations. The study shows that the impact of MVs on the objectives mass flow and total pressure is linear, while the isentropic efficiency is nonlinear with respect to surface imperfections.

Clark et al. [3] also evaluate the impact of surface imperfections on a transonic turbine stage using unsteady RANS computations to evaluate 105 optical rotor blade scans. The authors analyze each blade scan individually and as full annulus configuration consisting of 46 blades to quantify the unsteady interaction effects.

Based on the results from Clark, Brown et al. [4] use a Gaussian and linear regression surrogate model to predict the impact of MVs on the aerodynamic performance showing that a linear approximation method could be used for the assessment.

Other recent applications have shown that in order to overcome the high computational costs of 3D CFD RANS computation, the adjoint method is a less expensive alternative.

Zamboni et al. [5] show that an adjoint solver can be used to evaluate the impact of MVs using one coordinate measuring machine scan of a turbine rotor. The adjoint method can further be used as a quality management tool for turbine blade production as shown by Mulloth et al. [6]. Liefke et al. [7] have shown by using 102 optical turbine vane scans that the impact of MVs on the flow field is linear for mass flow and pressure loss. A further application of the adjoint methodology is presented by Luo and Liu [8] which use second order sensitivities. The authors apply a continuous adjoint Euler solver on a steam turbine stage evaluating the impact of MVs.

Until now all adjoint related publications have been single passage computations. This raises the question, whether the same principle can be applied to multi-passage simulations. Assuming that the MVs are small enough to not impact adjacent blade passages, the impact of the single-passages could be superpositioned to assess the impact of a multi-passage configuration. The MVs are thus considered small when they have a linear impact on the flow field.

Modeling a full annulus nonaxisymmetric blade row with 3D CFD, however, is computational too expensive for a daily use in an industrial context. A reduction from full annulus to multiple blade passages is consequently a first step to reduce the computational time for an impact evaluation of MVs. Therefore only two, four and eight vane passages are modeled to reduce the computational time.

The main aim of this paper is therefore to quantify the impact of MVs on a turbine stage using nonaxisymmetric multi-passage RANS simulations and to show that the adjoint method can be applied to achieve similar results, but at a lower computational cost.

The first part of this paper describes a turbine stage test case with a probabilistic multi-passage model to evaluate the impact of MVs. In the second part the results of the multi-passage RANS computations using two, four and eight passages are shown and discussed validating the single-passage superpositioning. The third part applies then the adjoint method to compute the aerodynamic impact for the single passages and the superpositioning of multiple passages. To validate the accuracy of the adjoint method, the results are compared to previous multi-passage RANS computations. Additionally the computational efficiency of using adjoint compared to RANS-based Monte Carlo simulations is outlined.

TEST CASE DESCRIPTION

The test case chosen for this paper is a first stage of heavy duty turbine close to a maximum power operating point. In order to preserve the proprietary informations of the geometry only scaled and normalized values are shown. In total a set of 102 turbine vane blades is analyzed using 3D optical white light scans, which have been previously used by Liefke et al. [7].

FIGURE 1: SCALED TURBINE STAGE WITH FOUR VANE PASSAGES [RED] AND ONE ROTOR PASSAGE [BLUE]

In comparison with [7] the previous single vane setup, however, has been extended to include the following blade row to model the aerodynamic impact more accurately. The rotor blade is kept as the original baseline geometry for all aerodynamic impact evaluations. The accuracy of the optical scans is between 10 to 35 μm, which is well below the blade surface tolerances and thus sufficiently accurate to model the MVs. Furthermore, the vane geometry includes blade fillets at hub and shroud to correctly replicate the MVs between blade surface and end-wall. Cooling features are not part of the setup to focus on the aerodynamic flow of the test case.

The first part of this section details the computational methods as well as the CFD domain of the single and multi-passage computations. In the second part the modeling of the MVs of the turbine vane is described. The third part outlines the probabilistic multi-passage model for two, four and eight vane passages.

Computational Methods

The mesh generation of the single-passage turbine stage is done using Autogrid 5. For the flow evaluations in this work the turbomachinery CFD suite Trace developed at the German Aerospace Center (DLR) is used. The MVs are imposed on the original baseline geometry by mesh morphing using Trace Prep [9], the pre-processor of Trace. The adjoint computations in the second part of the paper are performed using the algorithmically-differentiated (AD) version of Trace. AdjointTrace is a discrete adjoint flow solver which is based on reverse mode differentiation of the primal solver [10].

The adjoint method differentiates a CFD result in regard to a specific objective. This is especially computational efficient when evaluating numerous geometry variations. Since first order sensitivities are applied, the effect on the turbomachinery flow field must be small enough to be considered as linear.

At the inlet of the turbine stage a radial total pressure and temperature distribution together with an inlet flow angle is applied. For the outlet of the rotor blade a radial pressure distribution is set, while for the coupling of the vane and rotor a mixing plane approach is used. The fluid is assumed to behave as an ideal gas with adiabatic walls. The flow field is fully turbulent using the $k-\omega$ turbulence model [11] in conjunction with Kato-Launder's [12] stagnation anomaly fix. Furthermore the computational grid uses wall-functions with an average $y^+ \approx 25$. The stators mesh contains 440.000 nodes, while the rotor mesh contains 780.000 nodes. Both single and multi-passage domains use periodic boundary conditions in circumferential direction.

Manufacturing Variation Modeling

In this work a direct mesh morphing approach is used. The scanned MVs are measured by optical white light scans and then

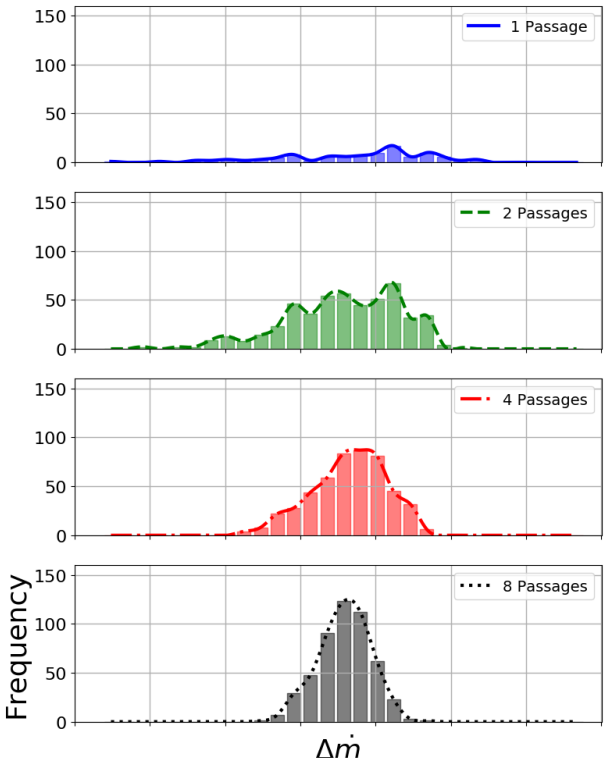

FIGURE 2: MASS FLOW HISTOGRAM FOR MULTIPLE PASSAGES

applied to the CFD setup of the baseline geometry. The MVs mapping process consists of four steps:

At first the surface imperfection of each blade scan, which stores the geometry data in an STL file format, are quantified using a 2D unstructured tetrahedral FEM mesh of the blade surface, calculating the distance in normal direction. Features such as cooling holes and cooling slots are, however, not included by selectively leaving out these parts during the finite element surface selection. As a second step the mesh nodes are moved individually using a cold to hot deformation vector field. The deformation is based on a FEM calculation from the baseline turbine vane, representing the geometry under "hot" loading conditions. Next the unstructured FEM mesh nodes are interpolated onto the structured CGNS surface geometry using a bilinear interpolation method. Finally the deformation is imposed by applying mesh morphing to move the surface nodes of the baseline blade surface onto the correct position. During the mesh morphing, however, the node deviations for nodes between 0-5% and 95-100% span are decreased linearly. This leads to a deformation of zero at 0% and 100%. This is done to prevent a step like edge feature near the hub and shroud fillet of the turbine vane. In total 102 deformed meshes are generated.

To validate the mesh morphing the Hausdorff distance between the morphed CGNS surface geometry and the optical scan

has been calculated for all 102 deformed meshes [13]. The Hausdorff distance calculates the maximum distance between two geometries. This means that the distance from each surface point from the optical blade scan to the CGNS blade surface and vice versa has been calculated. The maximum Hausdorff distance is located at the blade fillet and is below 180 μm. As a further note the maximum Hausdorff distance for the region of the blade surface is below 80 μm. For proprietary reasons the calculated Hausdorff distance over the blade surface is not displayed. Nevertheless, the modeling variations between the optical scan and CFD geometry are considered to be small enough to not impact the results.

Multi-Passage Modeling & Monte Carlo Setup

For the creation of the turbine stage multi-passage model, the vane block is duplicated and rotated to create identical multi-passages consisting of the baseline geometry. In a next step the CGNS skin block nodes of the vanes are replaced with skin block nodes from one of the 102 deformed CGNS files. During the node replacement only inner block nodes are moved, which do not share nodes with other CGNS blocks. This is done to prevent the creation of negative cells and to maintain the general CGNS block connectivity. A similar approach is presented by Lejon et al. [2]. The result is shown in Fig. 1 depicting a rotated and duplicated turbine stage with four vane passages. The picture has been distorted for proprietary reasons.

For the evaluations of aerodynamic scatter for multiple passages a Monte Carlo simulation for two, four and eight passages is performed with 500 evaluation each. This high number of 500 evaluations is chosen to guarantee a sufficient number of blade scan combinations for each passage as well as to reduce the statistical error of the Monte Carlo simulation. For each multi-passage model a number of multiple random CGNS deformation files is drawn and combined to produce the multi-passage setup. The random blade sampling is performed using the python module scipy [14].

As an additional reference the 102 single-passage deformations are also evaluated to compare to the multi-passage results. Thus, in total 1602 turbine stage computations are performed with the CFD solver Trace evaluating the multi-passage aerodynamic impact.

MULTI-PASSAGE RESULTS

This section presents the multi-passage results for one, two, four and eight vane passages of the heavy duty turbine stage using RANS computations. The first part shows the effect of multiple vane passages on the objectives mass flow and isentropic efficiency. In the second part the single passage gradient results are superpositioned to be compared with the multi-passage results.

TABLE 1: MULTI-PASSAGE NORMALIZED MEAN AND SCATTER VALUES

Objective	Passages	1	2	4	8
$\dot{m}$	μ_p/μ_1	1.0	0.9991	0.9995	0.9992
η	μ_p/μ_1	1.0	1.0000	1.0003	0.9997
$\dot{m}$	σ_p/σ_1	1.0	0.7355	0.5063	0.3682
η	σ_p/σ_1	1.0	0.6828	0.4716	0.3277

The mass flow is defined as

$$\dot{m} = \int \rho v \, dA \tag{1}$$

at the outlet of the stage using the area, density and absolute velocity. As second objective the isentropic efficiency is used which is defined as

$$\eta = \frac{H_{02} - H_{01}}{H_{02,is} - H_{01}} \tag{2}$$

using the total enthalpy at the inlet and outlet of the rotor blade. The efficiency objective thus evaluates the impact on the rotor efficiency for a variation of different inlet conditions caused by the upstream vane.

Due to intellectual proprietary reasons only the normalized delta objective values ΔF are shown which are defined as

$$\Delta F = \frac{F_{MultiPassage} - F_{Baseline}}{F_{Baseline}} \cdot 100 \quad with \quad F \in \{\dot{m}, \eta\} \tag{3}$$

The values are normalized using the single passage baseline computation results.

Effect of Multi-Passages

Figure 2 displays the mass flow deviation histogram for two, four and eight passages as well as for the single passage. While for each multi-passage simulation a total of 500 computations were conducted, the single-passage configuration evaluates the 102 deformed meshes directly. The figure shows that the scatter range of the mass flow decreases with an increase in the number of passages. This agrees with the previous results from Lange et al. [1] who observed the same for a compressor stage.

The MVs mostly impact the stagger angle and blade thickness of the blade, thereby altering the passage throat area and dictating the aerodynamic performance. While for an increase in

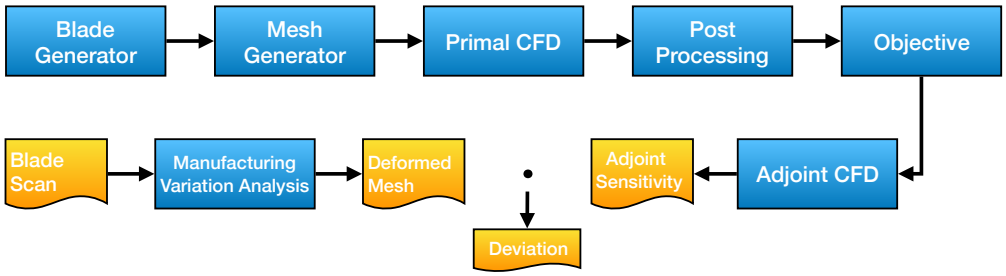

FIGURE 3: ADJOINT-BASED TOOLCHAIN FOR IMPACT EVALUATION

throat area the mass flow increases, the mass flow decreases for a reduction in throat area. A single-passage axisymmetric model therefore has a constant throat area, whereas a multi-passage model covers different variations in throat area. Figure 4 displays such a variation in throat area, depicting a nonaxisymmetric passage with two different blades.

For the isentropic efficiency objective of the rotor, on the other hand, the variation is caused by the varying trailing edge thickness of the modeled turbine vanes. A thicker trailing edge leads to an increase in pressure loss and thus to a lower total pressure at the inlet of the turbine rotor.

Table 1 shows the mean (μ) and standard deviation (σ) values for both objectives. The values are also normalized with the single-passage results. For mass flow and isentropic efficiency the mean values stay almost constant compared to the single passage results. Only the aerodynamic scatter reduces to around 37% and 33% for mass flow and isentropic efficiency when considering eight vane passages.

The reduction in standard deviation can be explained by the increase in blade passages. The impact when considering only one blade passage with surface imperfections gets amplified by the axisymmetric model. In a multi-passage simulation the possibility of combining multiple blades with a high magnitude of MVs are lower, therefore showing less amplification and a lower scatter range.

The lower aerodynamic scatter can be further be explained by the central limiting theorem (CLT) [15]. The CLT states that the normalized sum of independent modeled variations with a finite mean and variance tend towards a normal distribution. The normalized aerodynamic scatter can therefore be described as

$$\frac{\sigma_p}{\sigma_1} \approx \frac{1}{\sqrt{p}} \tag{4}$$

with p being the number of passages. Figure 5 shows the normalized standard deviation for the modeled blade passages and the CLT approximation. The CLT agrees very well with the computed normalized aerodynamic scatter for two, four and eight passages. For eight blade passages the scatter reduces to around 35%, which is a very good approximation for the com-

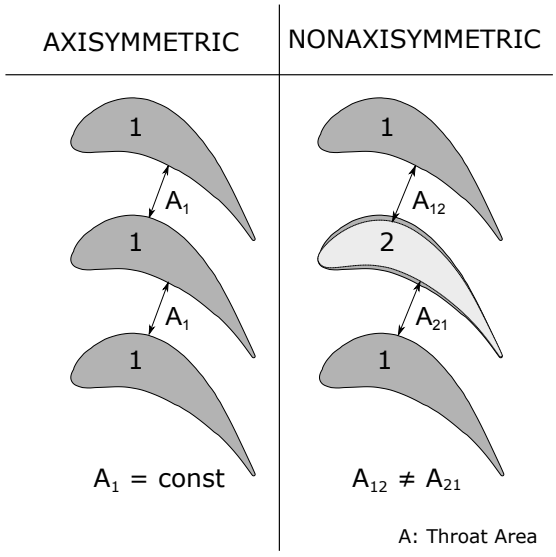

FIGURE 4: SKETCH AXISYMMETRIC & NONAXISYMMETRIC PASSAGE MODEL

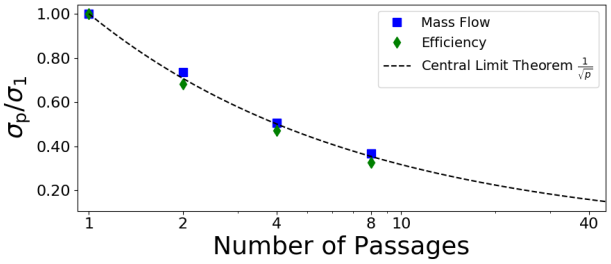

FIGURE 5: SEMI-LOGARITHMIC MULTI-PASSAGE MASS FLOW AND EFFICIENCY SCATTER

puted scatter results for mass flow and efficiency with 37% and 33%.

The applicability of the CLT confirms therefore the assumption of linear independent blade passages and provides a general zero parameter approximation method for the aerodynamic scatter. Thus showing that the empirical two parameter law proposed by Lange et al. [1] for the aerodynamic scatter prediction is not necessary.

Effect on Adjacent Passages

If the MVs are small enough to only affect the flow field of the individual blade passage, then the impact of multiple blade passages could be derived by superpositioning the individual effects. This would mean that the modeled MVs blade passages are linear independent. A nonaxisymmetric multi-passage modeling would then not be required.

To validate this assumption the single-passage impacts are going to be superpositioned and compared to the previous presented multi-passage results. Assuming the multi-passage model uses the blade scans A and B for the evaluation for a two passage model, then the computed single-passage mass flow from A and B are summed up and divided by the number of passages. For the superpositioned isentropic efficiency the single-passage efficiency value averaged with the passage mass flow is used. The superpositioned value of mass flow and isentropic efficiency are thus defined as

$$\dot{m}_{Superposition} = \frac{n}{p} \cdot \sum_{i}^{p} \dot{m}_i \quad and \tag{5}$$

$$\eta_{Superposition} = \frac{\dot{m}_{Superposition}}{p} \cdot \sum_{i}^{p} \frac{\eta_i}{\dot{m}_i} \tag{6}$$

with n being the number of blades in the blade row and p the number of modeled passages. Considering that the single-passage gradient computations use the axisymmetric approach the mass flow needs to be multiplied by the number of blades in the blade row to match the computed multi-passage mass flow.

The results for the mass flow comparison is shown in Fig. 6 for two, four and eight passages. Additionally the bisection is plotted indicating the linearity of the results. The superpositioned mass flow values agree very well with the multi-passage results. With an increase in passages the variability decreases and an almost identical mass flow is calculated. Only for the superposition with two passages the mass flow deviates slightly with an absolute deviation of less than 0.5% in mass flow. For an increased number of passages, however, this improves and the results match almost perfectly. The isentropic efficiency comparison is plotted in Fig. 7 showing a similar good agreement. Only the deviations for two passages are slightly higher with a maximum absolute deviation of 0.6%

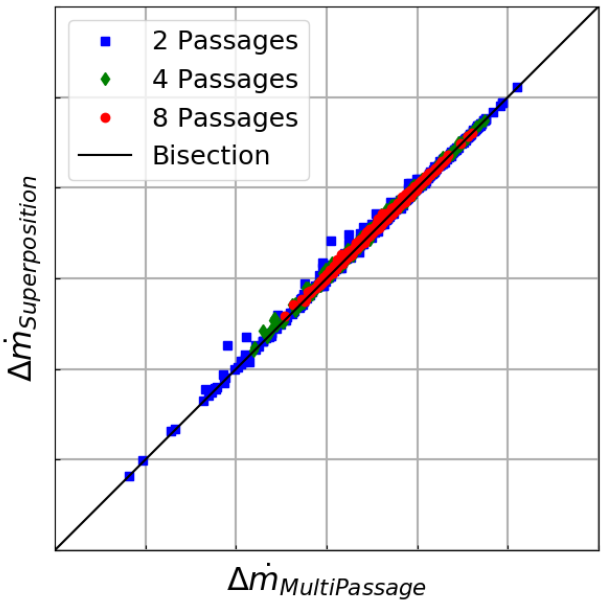

FIGURE 6: MASS FLOW GRADIENT SUPERPOSITION VS MULTI PASSAGE

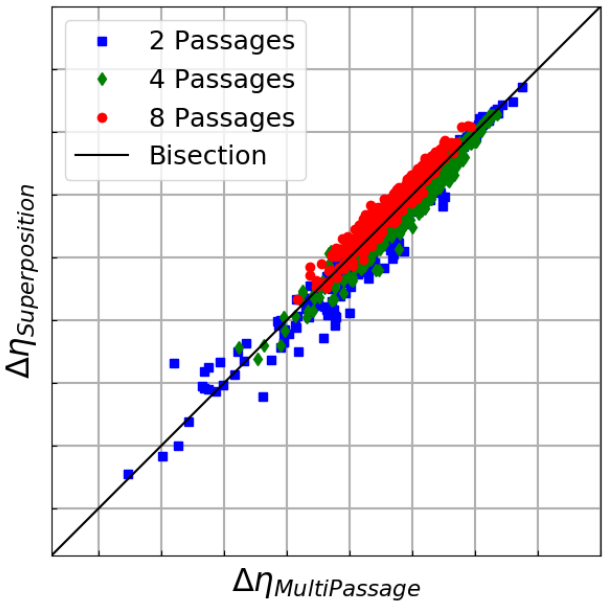

FIGURE 7: ISENTROPIC EFFICIENCY GRADIENT SUPERPOSITION VS MULTI PASSAGE

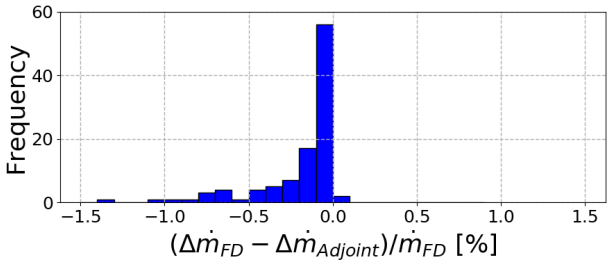

FIGURE 8: MASS FLOW ADJOINT GRADIENT DEVIATION IN REGARD TO FINITE DIFFERENCES

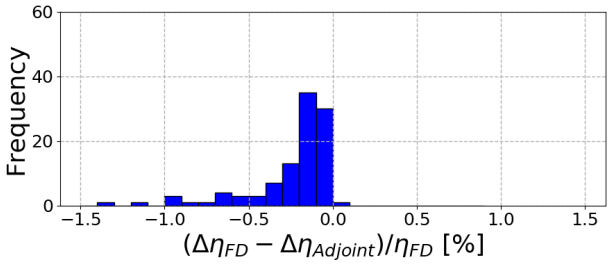

FIGURE 9: ISENTROPIC EFFICIENCY ADJOINT GRADIENT DEVIATION IN REGARD TO FINITE DIFFERENCES

The agreement of the superpositioned passages proves that the modeled MVs are small enough to not impact other adjacent passages. Therefore the need for nonaxisymmetric blade passage evaluations for MVs impact assessment is not necessary. As long as the surface imperfections are small enough to only effect the flow field in one blade passage, the impact can be evaluated by superpositioning alone. The previous mentioned variation in throat area for multiple passages is therefore small enough to be negligible.

Nevertheless, using 3D RANS computation to evaluate the impact of 102 optical blade scans is still computational expensive.

IMPACT EVALUATION WITH ADJOINT

Using the adjoint method to reduce the computational time of evaluating the impact of MVs would furthermore benefit the use as an industrial design tool. In this section the adjoint method is applied to quantify the impact of MVs on the aerodynamic performance of a heavy duty turbine stage. First an adjoint-based process tool chain is introduced to calculate the impact of MVs for a single-passage configuration. In the second part the adjoint gradients are then validated against finite differences. The third part describes the application of the adjoint gradients to the passage superposition and compares the results with the previous multi-passage RANS computations.

Adjoint Process Tool Chain

The process tool chain steps for an impact evaluation with adjoint is shown in Fig. 3. The evaluations starts with the blade generation and meshing of the baseline geometry. This is followed by a primal CFD RANS evaluation and a post processing step to calculate the required objective values of the baseline geometry. The next step is an adjoint CFD computation, which has to be run for each chosen objective to compute the objective sensitivities with regard to each mesh node.

These can then be used to multiply the 3D sensitivity field with a 3D surface deformation vector field. The vector field is thereby calculated from the baseline and a deformed mesh. The calculated impact is thus the sum of the product of the node sensitivity and node deformation vector. This process is then applied to the deformed mesh files producing the change in mass flow and efficiency for all 102 scanned blades.

The steps for the MVs analysis, as displayed in Fig, 3, are identical with the manufacturing variation modeling in the second section of this paper. These 102 calculated deviations are then used for the gradient superposition. The advantage of the adjoint method is, hence, that it scales with the number of objectives (2) and not with the number of shapes (102).

Single-Passage Adjoint Accuracy

To validate the basic assumption of linearity for the adjoint method, the adjoint gradients are compared to finite difference gradients, which have been previously calculated for the single-passage deviations results. The absolute gradient deviation is defined as

$$\frac{\Delta F_{Nonlinear} - \Delta F_{Adjoint}}{F_{Nonlinear}} \cdot 100 \quad with \quad F \in \{\dot{m}, \eta\} \tag{7}$$

to quantify the deviation between the nonlinear finite difference and the linear adjoint gradients. It is noted that the non-dimensionalization is not appropriate for efficiency, however, due to proprietary reasons this is done on purpose.

The absolute deviation histogram for the mass flow objective is shown in Fig. 8. It can be seen that the adjoint mass flow gradients agree very well with the finite differences. Around 10% of all 102 blade scans have an absolute deviation of more than 0.5%. For the isentropic efficiency objective the absolute deviations are shown in Fig. 9. Less than 10% of the blade scans have an absolute deviation of more than 0.75%, confirming the overall accuracy of the adjoint method.

Compared to the previous results from Liefke et al. [7], which used a single vane configuration, the results are comparable with most of the deviations being below 0.5% of the absolute baseline value in mass flow and efficiency. The adjoint gradi-

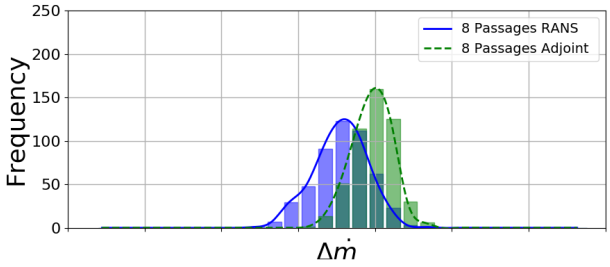

FIGURE 10: MASS FLOW HISTOGRAM FOR EIGHT PASSAGES WITH ADJOINT SUPERPOSITION RESULTS

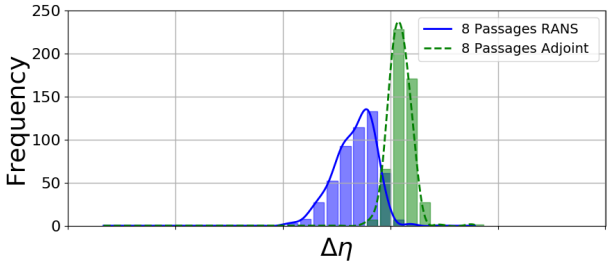

FIGURE 11: ISENTROPIC EFFICIENCY HISTOGRAM FOR EIGHT PASSAGES WITH ADJOINT SUPERPOSITION

ents are therefore considered accurate enough to be used for the multi-passage superposition in the next part.

Multi-Passage Adjoint Superposition

To compare the RANS-based mass flow with the adjoint superposition mass flow, the mass flow histogram for the eight passage model is shown in Fig. 10. For clarity reasons only the Monte Carlo results of the eight passage model are shown. The objective deviations are calculated as defined in Eq. 3. For the multi-passage objective values the eight passage RANS computations results are used, while the adjoint multi-passage results are calculated with Eq. 5 and Eq. 6.

The histogram shows an offset of around 0.2% for the mean mass flow value, which can be explained by the absolute deviation of the adjoint gradients. The mean value is therefore shifted by the constant deviations of the adjoint gradients causing the slight offset. For the standard deviation of the mass flow a decrease to 0.29 from 0.37 can be observed reducing the scatter range.

The same offset can be seen in Fig. 11 for the isentropic efficiency. Considering that the adjoint gradient absolute deviations are higher, this explains a higher offset of around 0.3% for the isentropic efficiency mean value. The scatter range, however, for the isentropic efficiency reduces from 0.33 to 0.17 compared to the single passage scatter. Using the adjoint superposition for efficiency would therefore underestimate the scatter by 17%.

Full Annulus Adjoint and RANS Superposition

The passage superposition approach also allows to assess furthermore the full annulus configuration. Therefore an additional Monte-Carlo simulation is setup, producing 500 full annulus vane-passage combinations of the turbine stage. The results of the scatter estimation for the 360° Monte Carlo model are displayed in Tab. 2.

The full annulus superpositioning is applied using adjoint and finite differences gradients from the single passage RANS evaluations. For the CLT only the first two decimals are approximated for proprietary reasons.

The mass flow aerodynamic scatter reduces to around 18% and 15% for the RANS and adjoint superpositioning respectively. For the isentropic efficiency, however, the scatter differs for both types of superpositioning with around 14% for the RANS and around 7% for the adjoint superpositioning. Thus reducing the underestimation of the adjoint-based efficiency scatter to around 6%. The insufficient adjoint accuracy for isentropic efficiency therefore prevents the use of adjoint for multi-passage superpositioning for this objective. It is noted that the difference between RANS-based and adjoint efficiency scatter deviates by around 50%. However, the main quantity of interest is the absolute scatter reduction and not the difference between both methods. The adjoint accuracy could further be improved by applying second order instead of first order sensitivities.

Compared to applying the CLT approximation, the superpositioning provides an objective specific aerodynamic scatter reduction value. Hence, for a general assessment of the scatter reduction the CLT is a sufficient approximation compared to RANS-based multi-passage simulations.

However, it should be noted that the application of the CLT is only valid if the individual passages can be superimposed. The nonaxisymmetric modeling of multiple blade passages using 3D CFD is therefore only required if the MVs have a magnitude level to effect adjacent passages.

Computational Efficiency

An overview of the conducted computations can be found in Tab. 3. The table is split between computations for the RANS-based Monte Carlo simulation and the adjoint computations. Additionally the table includes a CPU factor indicating the required time for each computation, the set residual limit for convergence and the total amount of time required.

The adjoint computation required an additional baseline computation to achieve a sufficient convergence level with a residual reduction below 10^{-6}. To achieve this level of convergence the CFL number has been continuously reduced to 1. The time for the baseline adjoint computation thus increases to a CPU time factor of around five.

TABLE 2: SUPERPOSITIONED FULL ANNULUS NORMALIZED SCATTER VALUES USING RANS & ADJOINT GRADIENTS

Objective	Passages	360°_{RANS}	$360^{\circ}_{Adjoint}$	360°_{CLT}
$\dot{m}$	σ_p/σ_1	0.1797	0.1528	≈ 0.15
η	σ_p/σ_1	0.1354	0.0705	≈ 0.15

Compared to the eight passage Monte Carlo simulation the adjoint approach outperforms the RANS-based approach by a factor of around 10. However, with the current adjoint run time the adjoint method is outperformed by the 102 single passage finite difference gradient superposition by a factor of around four. Nevertheless, in the context of an industrial blade casting process, where thousands of blades are produced, the computational superiority of adjoint becomes evident.

The adjoint method could therefore be applied for analyzing the casting quality of a turbine blade directly after production. The only additional costs at the manufacturing side would be the manufacturing variation analysis, the CFD geometry mesh morphing and the impact quantification through the adjoint dot product. An overview of these costs is shown in Tab. 4 using the previous CPU factor as normalization. Additionally the cost of applying a RANS-based impact quantification is shown to compare the RANS with the adjoint approach.

The MVs analysis and mesh morphing steps require the same computational time for both approaches. The main difference exists for the impact quantification for which the RANS approach needs around 100 times longer compared to adjoint approach. This is achieved by relying on the pre-computed adjoint sensitivity field to quantify the aerodynamic impact. The adjoint approach thus outperforms the RANS approach.

CONCLUSION

In this paper, the impact of MVs on a heavy duty transonic turbine stage has been analyzed using nonaxisymmetric multi-passage modeling. In total 102 optical white light scans of a turbine vane have been used to create Monte Carlo setups of two, four and eight vane passages to simulate the effect of nonaxisymmetric blading. The impact on mass flow and isentropic efficiency has been quantified showing that the aerodynamic mean value of the analyzed 102 single passage does not differ when considering multiple passages.

However, the aerodynamic scatter reduces up to 37% for mass flow and 33% for isentropic efficiency, when considering eight vane passages, compared to the single passage scatter. A similar scatter reduction can also be estimated based on the central limit theorem using the number of passages, which leads for eight passages to a reduction of $\frac{1}{\sqrt{8}} \approx 35\%$.

TABLE 3: OVERVIEW COMPUTATIONAL TIME FOR IMPACT QUANTIFICATION WITH RANS AND ADJOINT

Description	Residual	Number	CPU Factor	Total
Baseline	10^{-5}	1	1.00	1
1-Passage	10^{-5}	102	1.00	102
2-Passage	10^{-5}	500	1.66	830
4-Passage	10^{-5}	500	4.69	2345
8-Passage	10^{-5}	500	8.38	4190
Baseline Adjoint	10^{-6}	1	4.78	4.8
Adjoint	10^{-4}	2	197.40	394.8

The modeled MVs are small enough to only impact the flow field of a single passage. This allows to superimpose the single passage results linearly to simulate the same multi-passage impact. The need for an nonaxisymmetric multi-passage modeling is therefore only required, when the MVs have a magnitude level large enough to effect adjacent passages. The impact of multiple passages can therefore be computed by superpositioning the individual 102 aerodynamic impacts.

Therefore an adjoint impact tool chain has been used to reduce the computational time of evaluating the impact of the 102 blade scans. It has been shown that the absolute deviation for both objectives is below 0.5% for over 90% of all blade scans. The adjoint gradients have further been used for the multi-passage impact superpositioning for a full annulus blade passage. Thereby, proving that the aerodynamic scatter of the mass flow can be estimated correctly compared to the CLT full annulus RANS results, while the isentropic efficiency scatter reduction was underestimated by 6%.

The applicability of the adjoint method depends on the magnitude of the MVs as well as on the turbomachinery flow conditions. These should therefore be considered before applying the adjoint approach. While the computational superiority of adjoint could not be shown for the set of 102 blade scans. The superiority becomes apparent, when considering adjoint for the analysis of an industrial blade casting process outperforming a RANS approach by around 100 times.

ACKNOWLEDGMENT

The permission of Siemens AG to publish the results is greatly acknowledged.

A. Liefke and H. Gottschalk acknowledge partial financial

TABLE 4: OVERVIEW COMPUTATIONAL TIME FOR ANALYZING CASTING QUALITY WITH RANS AND ADJOINT

Analysis Step	RANS Approach	Adjoint Approach
MVs Analysis	0.0013	0.0013
Mesh Morphing	0.0057	0.0057
Impact Quantification	1.0000	0.0019
Total	1.0070	0.0089

support from the GIVEN project, grant no. 05M18PXA "Mathematics for Innovation" by the Federal Ministry of Education and Research (BMBF).

REFERENCES

[1] Lange, A., Voigt, M., Vogeler, K., Schrapp, H., Johann, E., and Gümmer, V., 2012. "Impact of manufacturing variability and nonaxisymmetry on high-pressure compressor stage performance". *Journal of Engineering for Gas Turbines and Power*.

[2] Lejon, M., Andersson, N., Ellbrant, L., and Martensson, H., 2018. "The impact of manufacturing variations on performance of a transonic axial compressor rotor". *ASME Turbo Expo 2018: Turbine Technical Conference and Exposition*.

[3] Clark, J. P., Beck, J. A., Kaszynski, A. A., Still, A., and Ni, R.-H., 2017. "The effect of manufacturing variations on unsteady interaction in a transonic turbine".

[4] Brown, J. M., Beck, J., Kaszynski, A., and Clark, J., 2018. "Surrogate modeling of manufacturing variation effects on unsteady interactions in a transonic turbine". *ASME Turbo Expo 2018: Turbine Technical Conference and Exposition*.

[5] Zamboni, G., Banks, G., and Bather, S., 2016. "Gradient-based adjoint and design of experiment cfd methodologies to improve the manufacturability of high pressure turbine blades". In ASME Turbo Expo 2016: Turbine Technical Conference and Exposition.

[6] Mulloth, A., Banks, G., Zamboni, G., and Bather, S., 2018. "A high fidelity quality assessment of high pressure turbine blades using surface curvature and gradientbased adjoint". *ASME Turbo Expo 2018: Turbine Technical Conference and Exposition*.

[7] Liefke, A., Marciniak, V., Janoske, U., and Gottschalk, H., 2018. "Using adjoint cfd to quantify the impact of manufacturing variations on a heavy duty turbine vane". In 7th European Conference on Computational Fluid Dynamics (ECCOMAS CFD 2018).

[8] Luo, J., and Liu, F., 2018. "Statistical evaluation of performance impact of manufacturing variability by an adjoint method". *Aerospace Science and Technology, 77*, pp. 471–484.

[9] Voigt, C., Frey, C., and Kersken, H., 2010. "Development of a generic surface mapping algorithm for fluid-structure-interaction simulations in turbomachinery". In 5th European Conference on Computational Fluid Dynamics (ECCOMAS CFD 2010).

[10] Backhaus, J., Schmitz, A., Frey, C., Mann, S., Nagel, M., Sagebaum, M., and Gauger, N. R., 2017. "Application of an algorithmically differentiated turbomachinery flow solver to the optimization of a fan stage". In 18th AIAA/ISSMO Multidisciplinary Analysis and Optimization Conference.

[11] Wilcox, D. C., 1988. "Reassessment of the scale-determining equation for advanced turbulence models". *AIAA journal*.

[12] Kato, M., 1993. "The modeling of turbulent flow around stationary and vibrating square cylinders". In Ninth Symposium on Turbulent Shear Flows, 1993.

[13] Weisstein, E. W., 2018. From mathworld –a wolfram web resource. hausdorff measure. [Online; http://mathworld.wolfram.com/HausdorffMeasure.html; accessed 25.01.2019].

[14] Jones, E., Oliphant, T., Peterson, P., et al., 2001–. SciPy: Open source scientific tools for Python. [Online; http://www.scipy.org/; accessed 25.01.2019].

[15] Weisstein, E. W., 2018. From mathworld –a wolfram web resource. central limit theorem. [Online; http://mathworld.wolfram.com/CentralLimitTheorem.html; accessed 25.01.2019].

